Solving PDEs With Spatial & Time Varying Coefficients: Dirac Wavefunction Passes Thru EM Wave

A. J. Kalinowski*[1]
[1]Consultant
*Corresponding author: East Lyme CT 06333, kalinoaj@aol.com

Abstract: COMSOL is used for obtaining the quantum mechanics wavefunction $\{\Psi_n(x,y,z,t)\}$ as a solution to the *time dependent* Dirac equations while determining the effect of a preexisting electromagnetic traveling wave (represented by a combined magnetic vector potential $\bar{\mathbf{A}}$ field and scalar electric potential ϕ field) on the propagating wavefunction. The probability evaluation of a particle being at a spatial point can be treated by the "wavefunction formulation" and is employed herein because it involves solving field PDEs, thus is directly adaptable to COMSOL.

Keywords: Quantum Mechanics, Time Dependent Dirac Equation, Wave Propagation.

1. Introduction

The paper illustrates the use of COMSOL for obtaining the quantum mechanics wavefunction $\{\Psi_n(x,y,z,t)\}$ (representing *matter waves*) as a solution to the *time dependent* Dirac equations. These equations are employed in particle physics and historically provided the first combined application of quantum mechanics and relativity theory by introducing a four component wavefunction $\{\Psi_n\}$, n=1,..4. Historically, $\{\Psi_n\}$ described the behavior of fermion type particles (e.g., electrons) and further predicted the existence of antiparticles (e.g., positrons) even before they were observed experimentally. COMSOL® Usage: the *General-Form PDE* "*time dependent*" study is employed. Archive Refs. [1-4] solve for Quantum Mechanics Dirac wavefunctions; however, this is the first COMSOL application towards solving the *time dependent* Dirac equations for particles in the presence of a preexisting traveling electromagnetic wave field. It is an extension of Ref.[4] that treated solutions in the presence of either a preexisting static electric field alone or magnetic field alone.

2. Governing Equations/Theory

Governing equations for the behavior of a free fermion particle of mass $\mathbf{m}$ in the presence of a magnetic and electric field, are represented by the *time dependent* quantum mechanics Dirac equations (with wavefunctions $\{\Psi_n(x,y,z,t)\}$ as the dependent variables) and are given by Ref.[5]:

$$\begin{aligned}
&\frac{1}{c}\frac{\partial\Psi_1}{\partial t}+\frac{\partial\Psi_4}{\partial x}-i\frac{\partial\Psi_4}{\partial y}+\frac{\partial\Psi_3}{\partial z}+i\Psi_1(\Phi+M)\\
&+i(i\mathbf{A}_y\Psi_4-\mathbf{A}_z\Psi_3-\mathbf{A}_x\Psi_4)=0\\
&\frac{1}{c}\frac{\partial\Psi_2}{\partial t}+\frac{\partial\Psi_3}{\partial x}+i\frac{\partial\Psi_3}{\partial y}-\frac{\partial\Psi_4}{\partial z}+i\Psi_2(\Phi+M)\\
&+i(A_z\Psi_4-\mathbf{A}_x\Psi_3-i\mathbf{A}_y\Psi_3)=0 \qquad (1)\\
&\frac{1}{c}\frac{\partial\Psi_3}{\partial t}+\frac{\partial\Psi_2}{\partial x}-i\frac{\partial\Psi_2}{\partial y}+\frac{\partial\Psi_1}{\partial z}+i\Psi_3(\Phi-M)\\
&+i(i\mathbf{A}_y\Psi_2-\mathbf{A}_z\Psi_1-\mathbf{A}_x\Psi_2)=0\\
&\frac{1}{c}\frac{\partial\Psi_4}{\partial t}+\frac{\partial\Psi_1}{\partial x}+i\frac{\partial\Psi_1}{\partial y}-\frac{\partial\Psi_2}{\partial z}+i\Psi_4(\Phi-M)\\
&+i(\mathbf{A}_z\Psi_2-\mathbf{A}_x\Psi_1-i\mathbf{A}_y\Psi_1)=0
\end{aligned}$$

where $\mathbf{m}$=particle mass, c= light speed , $\mathbf{e}$=particle charge, $\hbar$ =h/(2π), (*h* is Planck's constant), i=√(-1)

$$\begin{aligned}
&\textit{with}\quad \mathbf{A}_x\equiv A_x\mathbf{e}/\hbar \quad \mathbf{A}_y\equiv A_y\mathbf{e}/\hbar \quad \mathbf{A}_z\equiv A_z\mathbf{e}/\hbar \quad M\equiv \mathbf{m}c/\hbar\\
&\Phi\equiv \mathbf{e}\phi/(c\hbar) \quad \bar{\mathbf{B}}=\nabla\mathbf{x}\bar{\mathbf{A}} \quad \bar{\mathbf{E}}=-\nabla(\Phi)-\partial\bar{\mathbf{A}}/\partial t \qquad (2)
\end{aligned}$$

Equations(2) relate the normalized vector potential $\bar{\mathbf{A}}$ and scalar potential Φ to the normalized vector magnetic $\bar{\mathbf{B}}$ field and electric $\bar{\mathbf{E}}$ field ($\bar{A}$ & ϕ are unnormalized).

2.1 Two-D *time dependent* form

A 2-D form of governing Eqs.(1) are solved for in *time dependent* problems using the COMSOL MULTIPHYSICS® General-Form PDE "T*ime dependent*" studies option. Two dimensional solutions are sought where the wavefunction depends on spatial coordinates x,y. Thus setting A_z=0 and letting Ψ_n gradients in the z direction drop out, leads to the 2-D form of Eqs.(1) which are the following pair of pde's Eqs.(4a-b) and pair Eqs.(5a-b). In Eqs.(4a-b) and Eqs.(5a-b), nice sized quantities are experienced during the computation process, by using *primed* non-dimensional independent variables and corresponding PDE parameters, as defined by Eqs.(3). The selection of scale values for $\{\mathbf{T},\mathbf{L}\}$ is

treated later in **2.3**. The Eqs.(4a-b) in terms of $\{\Psi_1(x',y',t'),\Psi_4(x',y',t')\}$ *are uncoupled* from the

$$t' \equiv t/\mathbf{T},\ x' \equiv x/\mathbf{L},\ y' \equiv y/\mathbf{L},\ c' \equiv c\mathbf{T}/\mathbf{L},\ \bar{\mathbf{A}}' \equiv \bar{\mathbf{A}}\mathbf{L},\ \bar{\mathbf{E}}' \equiv \bar{\mathbf{E}}\mathbf{L}^2$$
$$M' \equiv M\mathbf{L},\ \omega' \equiv \omega\mathbf{T},\ \Phi' \equiv \Phi\mathbf{L},\ \mathcal{A}' \equiv \mathcal{A}\mathbf{L},\ \bar{\mathbf{B}}' \equiv \bar{\mathbf{B}}\mathbf{L}^2 \quad (3)$$

Eqs.(5a-b) that are in terms of $\{\Psi_2,\Psi_3\}$. Except for the M′ sign, Eq.(4a) is just like Eq.(5a) and Eq. (4b) is just like Eq.(5b) where $\Psi_1 \leftrightarrow \Psi_3$ & $\Psi_4 \leftrightarrow \Psi_2$ .Thus the solution procedure for solving

$$\frac{1}{c'}\frac{\partial\Psi_1}{\partial t'}+\frac{\partial\Psi_4}{\partial x'}-i\frac{\partial\Psi_4}{\partial y'}+i(\Phi'+M')\Psi_1-i\mathcal{A}'^*\Psi_4=0 \quad (4a)$$
$$\frac{1}{c'}\frac{\partial\Psi_4}{\partial t'}+\frac{\partial\Psi_1}{\partial x'}+i\frac{\partial\Psi_1}{\partial y'}+i(\Phi'-M')\Psi_4-i\mathcal{A}'\Psi_1=0 \quad (4b)$$
$$\frac{1}{c'}\frac{\partial\Psi_3}{\partial t'}+\frac{\partial\Psi_2}{\partial x'}-i\frac{\partial\Psi_2}{\partial y'}+i(\Phi'-M')\Psi_3-i\mathcal{A}'^*\Psi_2=0 \quad (5a)$$
$$\frac{1}{c'}\frac{\partial\Psi_2}{\partial t'}+\frac{\partial\Psi_3}{\partial x'}+i\frac{\partial\Psi_3}{\partial y'}+i(\Phi'+M')\Psi_2-i\mathcal{A}'\Psi_3=0 \quad (5b)$$
$$where\ \mathcal{A}'(x,y) \equiv \mathbf{A}'_x+i\mathbf{A}'_y\ ;\quad \mathcal{A}'^*(x,y) \equiv \mathbf{A}'_x-i\mathbf{A}'_y \quad (6)$$

Eqs.(4a-b) are just like solving Eqs.(5a-b), thus we focus on solving $\{\Psi_1(x',y',t'),\Psi_4(x',y',t')\}$.

2.2 Governing equations in presence of combined electric potential Φ′ field and magnetic $\bar{\mathbf{A}}'$ field

The alternate second order form of simultaneous Eqs.(4a-b) is given as Eqs.(7a-b) and has shown to be computationally robust, where the

$$\frac{\partial^2\Psi_1}{\partial x'^2}+\frac{\partial^2\Psi_1}{\partial y'^2}-\frac{1}{c'^2}\frac{\partial^2\Psi_1}{\partial t'^2}+(C_1(x',y',t')-M'^2)\Psi_1+C_2(x',y',t')\frac{\partial\Psi_1}{\partial t'}$$
$$+C_3(x',y',t')\frac{\partial\Psi_1}{\partial x'}+C_4(x',y',t')\frac{\partial\Psi_1}{\partial y'}+C_5(x',y',t')\Psi_4=0 \quad (7a)$$

$$\frac{\partial^2\Psi_4}{\partial x'^2}+\frac{\partial^2\Psi_4}{\partial y'^2}-\frac{1}{c'^2}\frac{\partial^2\Psi_4}{\partial t'^2}+(\hat{C}_1(x',y',t')-M'^2)\Psi_4+\hat{C}_2(x',y',t')\frac{\partial\Psi_4}{\partial t'}$$
$$+\hat{C}_3(x',y',t')\frac{\partial\Psi_4}{\partial x'}+\hat{C}_4(x',y',t')\frac{\partial\Psi_4}{\partial y'}+\hat{C}_5(x',y',t')\Psi_1=0 \quad (7b)$$

C_i, $\hat{C}_i$ coefficients are in terms of the known electric and magnetic potentials, namely:

$$C_1=-\frac{i}{c'}\frac{\partial\Phi}{\partial t'}+\Phi^2-i\frac{\partial\mathcal{A}'}{\partial x'}-\frac{\partial\mathcal{A}'}{\partial y'}-\mathcal{A}'\mathcal{A}'^*\ ;C_2=-2i\Phi/c' \quad (7c)$$
$$C_3=-2i\mathbf{A}'_x;\ C_4=-2i\mathbf{A}'_y;\ C_5=\frac{i}{c'}\frac{\partial\mathcal{A}'^*}{\partial t'}+i\frac{\partial\Phi}{\partial x'}+\frac{\partial\Phi}{\partial y'}$$
$$C_7=i\left(\frac{\partial\Phi}{\partial t'}-M'-\frac{\omega}{c'}\right)$$
$$\hat{C}_1=-\frac{i}{c'}\frac{\partial\Phi}{\partial t'}+\Phi^2-i\frac{\partial\mathcal{A}'^*}{\partial x'}+\frac{\partial\mathcal{A}'^*}{\partial y'}-\mathcal{A}'\mathcal{A}'^*\ ;\hat{C}_2=-2i\Phi/c' \quad (7d)$$
$$\hat{C}_3=-2i\mathbf{A}'_x;\ \hat{C}_4=-2i\mathbf{A}'_y;\ \hat{C}_5=\frac{i}{c'}\frac{\partial\mathcal{A}'}{\partial t'}+i\frac{\partial\Phi}{\partial x'}-\frac{\partial\Phi}{\partial y'}$$

The Eq.(7a) is obtained by first summing $-i\partial/\partial y'$ of Eq.(4b) + $\partial/\partial x'$ of Eq.(4b) and then using Eq.(4a) to eliminate the [$\partial\Psi_4/\partial x' - i\partial\Psi_4/\partial y'$] term in that sum. Next the remaining $\partial\Psi_4'/\partial t'$ coupling term is eliminated using Eq.(4b). Equation (7b) is obtained by similarly operating on Eq.(4a) and using Eq.(4a) to eliminate the $\partial\Psi_1'/\partial t'$ term.

Alternate Eqs.(7a-b) have some advantages over Eqs.(4a-b), namely: a) the underlying wave propagation nature of these equations is evident via the embedded classical wave equation appearing in the first three terms, b) they appeared more computationally stable over long time integration histories, c) ease of applying normal derivative boundary conditions (e.g. those found in zero gradient boundary conditions or in absorbing boundary BC's), and d) unlike Eqs.(4a-b) these equations are uncoupled when the potentials are not present (Φ′=0, $\bar{\mathbf{A}}'$=0), where then, each one takes on the form of the relativistic Klein-Gordon Equation.

Local Steady State PDE for Ψ_1': The local PDE (i.e. temporarily holding independent variables {x′=x′, y′=y′, t′=t′} constant in the $C_i(x',y',t')$, $\hat{C}_i(x',y',t')$ coefficients in Eqs.(7a-b)) for the Ψ_1 wavefunction will be useful in predetermining the effect of the Φ′ and $\bar{\mathbf{A}}'$ potentials on an otherwise propagating free field Dirac wavefunction. Substituting Eqs.(8) into Eqs.(7a-b) (where

$$\Psi_n(x',y',t')=\psi_n(x',y',\omega')e^{-i\omega' t'}\ \ n=1\ or\ 4 \quad (8)$$

$C_i(x',y',t')$, $\hat{C}_i(x',y',t')$ are locally held constant) and after eliminating the ψ_4 in Eq.(7a) by using Eq. (4b), the following local uncoupled steady state Eq.(9) PDE is obtained for ψ_1 :

$$\nabla^2\psi_1+k_s'^2\psi_1+(C_3-\frac{C_5}{C_7})\frac{\partial\psi_1}{\partial x'}+(C_4-\frac{C_5}{C_7})\frac{\partial\psi_1}{\partial y'}=0 \quad (9)$$
$$k_D'^2=(\frac{\omega'}{c'})^2-M'^2;\quad k_s'^2=k_D'^2+C_1-i\omega'C_2+\frac{i\mathcal{A}'C_5}{C_7} \quad (10)$$
$$\lambda_s'(x',y',t') \equiv real\ pt\,(2\pi/k_s') \quad (11)$$

The first two terms in Eq.(9) are the Helmholtz equation where the k'^2_s term corresponds to the wave number squared and $\lambda'_s(x',y',t')$ corresponds to the wave length at local point (x′,y′,t′) . Note that the second of Eqs.(10) reduces to the freely propagating Dirac wavenumber k'^2_D when the EM potentials are turned off. Equation (9) is not solved herein, but rather is used establish the k'^2_s term which is used for the following reasons; (1) help select the strength of the EM field later on, (2) establish the influence of C_i coefficients relative to the squared freely propagating Dirac wave number k'^2_D and (3) for harmonically driven problems, obtain an estimate of the Ψ_1 spatial wave length

via Eq.(11), for FEM mesh size selection. Carpet plots of Eq.(11) over the integration spacial domain (x',y') for a fixed, t' shows where finer meshes are likely needed.

Φ′, Ā′ potential selection for EM wave in +y′ direction : A plane EM wave traveling in the +y′ direction has scalar and vector potentials given by Eqs.(12a-b) Ref.[6]:

$$\Phi' = -(x' - x_0')E_0' Cos(\tilde{k}'y' - \tilde{\omega}'t') \quad E_0' = const. \qquad (12a)$$
$$A_x' = 0;\ A_y' = -(x' - x_0')E_0' Cos(\tilde{k}'y' - \tilde{\omega}'t');\ A_z' = 0 \qquad (12b)$$

which correspond (via Eqs.(2)) to the constant amplitude electric and magnetic field vectors:

$$E_x' = E_0' Cos(\tilde{k}'y' - \tilde{\omega}'t');\ E_y' = 0;\ E_z' = 0 \qquad (13a)$$
$$B_x' = 0;\ B_y' = 0;\ B_z' = -E_0' Cos(\tilde{k}'y' - \tilde{\omega}'t') \qquad (13b)$$
$$\tilde{k}' \equiv \tilde{k}L \quad \tilde{\omega}' \equiv \tilde{\omega}'T \quad \eta \equiv \tilde{\omega}'/\omega' \quad \tilde{k}' = \eta\ \omega'/c' \qquad (13c)$$

where x_0' is the offset distance defining the start of the EM field. The primed EM wave frequency $\tilde{\omega}'$ is selected as η fraction of the driver frequency ω′ via the 3d Eq.(13c). The corresponding k′ EM wave number is from the 4th Eq.(13c) .

Φ′, Ā′ potential selection for EM wave in +x′ direction : For a plane EM wave traveling in the +x′, interchange x′ & y′ in Eqs.(12a-b) (also interchange x′ & y′ component subscripts in Eqs.(12b).

The size of E_0' is selected large enough to feel the influence of the EM field on $\Psi_1(x',y',t')$ yet small enough to allow the wavefunction solution to continue on as a propagating wave by comparing term sizes in the local steady state wave number squared $k_s'^2$. Next substitute Eqs.(12a-b) into Eq. (10) and keeping the two leading terms gives:

$$k_s'^2 \approx k_D'^2 + E_0' Cos(\tilde{k}'y' - \tilde{\omega}'t') 2\omega'(x' - x_0')/c' \qquad (14)$$
$$and\ defining \quad E_0' \equiv \alpha_E k_D'^2 \qquad (15)$$
$$k_s'^2 \approx k_D'^2 [1 + \alpha_E Cos(\tilde{k}'y' - \tilde{\omega}'t') 2\omega'(x' - x_0')/c'] \qquad (16)$$

where via Eq.(15), the size of E_0' is made relative to an α_E fraction of $(k_D')^2$. For example in the later Fig.(3) model, selecting α_E = .00477, the Eq.(16) 2nd term is .40 compared to 1 after the wave travels 5 waves into the EM field thus resulting a shorter wave length relative to the λ_D free field Dirac PW . The Eq.(16) Cos( ) ±1 variations cause $k_s'^2$ to be bigger or smaller than $(k_D')^2$ resulting in a smaller or bigger λ_s' wavelength compared to the λ_D' wavelength which in turn affects the required FEM mesh size.

2.3 Selection of drive frequency ω and non-dimensionalization parameters {T,L}

Frequency selection: De Broglie's photon-to-particle extension of Planck's relation between particle energy E_p and angular frequency ω (i.e. $E_p = \hbar\omega$), along with the *relativistic* relation between E_p and velocity [5], $E_p = mc^2/\sqrt{(1-\beta^2)}$, gives Eq.(17) for selecting the frequency in terms of the particle velocity v_p via the speed parameter $\beta = v_p/c$.

$$\omega = E_p/\hbar = cM/\sqrt{1-\beta^2}\ ; \quad \beta = v_p/c \qquad (17)$$

Non-dimensionalization {T,L} selection: The scale of QM is such that the numerical size of both time and space variables are extremely small in CGS units. Equations (4a-b), in the non-dimensional prime variables, are valid for *any* unit consistent values of {T,L}, however a convenient choice is to use the time period T_p and wave length λ_D of a propagating Dirac Equation plane wave (in the absence of EM fields). The size of all of the *primed variables* in the FEM models (both in model building, solving, and post processing) are then nice size numbers. Unprimed Eq.(18) represents the SS (steady state) wavefunctions

$$\Psi_n(x,y,t) = \psi_n(x,y,\omega)e^{-i\omega t} \quad n = 1\ or\ 4 \qquad (18)$$

where the SS exact solution to *unprimed* Eqs.(4a-b), for a PW of frequency ω, traveling in the +x dir., is given by Ref.[5] :

$$\begin{Bmatrix}\psi_1\\ \psi_4\end{Bmatrix} = A\begin{Bmatrix}1\\ 1/R\end{Bmatrix} exp[ik_D x] \qquad (19)$$
$$k_D = \sqrt{(\omega/c)^2 - M^2};\ R = \frac{k_D}{(\omega/c) - M} \qquad (20)$$

where A is an arbitrary constant. Therefore after selecting driver frequency ω, the following scale values for {T,L} are defined by:

$$T \equiv 2\pi/\omega \quad L = 2\pi/k_D = 2\pi/\sqrt{(\omega/c)^2 - M^2} \qquad (21a)$$
$$\text{and primed } \omega', k_D' \text{ are: } \omega' = \omega' T \quad k_D' = k_D L \qquad (21b)$$

3. Method

A bounded EM traveling wave is embedded in a larger domain where the startup zone has a zero EM field. This is accomplished by applying COMSOL's "*STEP* functions" (with gradual cubic ∫ shaped rise) to the E_0' terms (via $\mathcal{A}'$ and Φ′) that appear in Eqs.(4a-b and Eqs.(7a-d). The Dirac equations are solved in the time domain by driving an upfield face of a model (that is initially at a zero wavefunction state) with exp(-iω′t′) harmonic loadings, and then track the transient waves that propagate towards the downfield end of the model.

3.1 FEM Boundary Conditions

3.1.1 FEM Wave Generation Driven Surface: transient solutions are generated by driving the upfield surfaces with time harmonic loadings of the form:

$$\Psi_n(x'_s,y'_s,t') = \psi_n(x'_s,y'_s) f(t') e^{-i\omega' t'} \; n = 1,4 \quad (22)$$

where $f(t')$ is a gradual time increasing multiplier on the harmonic driver and $\psi_n(x'_s,y'_s)$ is the wavefunction distribution (from a free field PW or CylW) at surface points $\{x'_s,y'_s\}$. This gradual increase is to help minimize any suddenly applied loading effects (see Ref.[4] for $f(t')$ formula). The $f(t')$ exponentially increases from ε_0 to 1.0 over N_c time cycles. The Ψ_1 input driver, using ε_0 =.05 and N_c =6, is shown in Fig.(1a) (Ψ_4 is a similar shape). In Fig.(1b), the FFT of the real part of the Ψ_1 driver shows a dominant primed frequency at f′=1.0 .

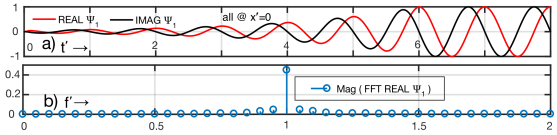

Figure 1. FEM Wave Generation Driver (Ψ_1)

3.1.2 FEM Model Termination Surfaces:

(i) absorbing BC : not used here; the computations are halted just before the wave meets the outer boundary.

(ii) zero value BC : this is used down field of the propagation at the outer boundary points $\{x_b',y_b'\}$ of the model, namely $\Psi_n(x_b',y_b',t')=0$

(iii) normal gradient BC: normal grad. $\vec{n}\bullet\nabla\Psi_n(x'_b,y'_b,t')=0$, @ surface points $\{x_b',y_b'\}$, where $\vec{n}$ is a surface unit normal vector and is used with Eqs.(7a-b) at wave guide transverse cuts.

3.2 FEM Initial Conditions

The FEM model is started from rest throughout the entire spatial domain $\mathcal{D}$, therefore:

$$\Psi_n(x',y',0)=0\,;\; \frac{\partial\Psi_n(x',y',0)}{\partial t'}=0 \;\; all\; x',y' \text{ in } \mathcal{D} \quad (23)$$

It is noted that because of the manner Eq.(22) is constructed, evaluating it at t'=0 is consistent with Eqs.(23) for both $\Psi_n(x'_s,y'_s,0)$ and $\partial\Psi_n(x'_s,y'_s,0)/\partial t'$.

3.3 Probability Density Computation

The probability density $\rho(x',y',t')$ is defined as the probability per unit area of the particle being at a particular spatial point $\{x',y'\}$, and is given by Eq.(24) Ref.[5].

$$\rho(x',y',\omega') = |\Psi_1|^2 + |\Psi_4|^2 \quad (24)$$

3.4 Model Parameters

The primed physical parameters in the PDEs coefficients Eqs.(7c-d) (M', c', $\mathcal{E}'_0$, $\tilde{\omega}'$) are governed by the previously defined $\{\beta, \alpha_E, \eta\}$ ratios.

4. EM Traveling wave Potential Φ', $\bar{A}'$ Field Results

The basic building blocks of the Dirac theory are freely propagating matter waves such as planar ones. Exact validation solutions to these wave propagation problems (when the time & spatial varying Φ', $\bar{A}'$ potentials are present) are not generally possible, even for simple 1-D propagation. Instead COMSOL comparisons to the same problem solved by alternate FEM code (e.g. Mathematica™) is made.

4.1 Bar Plane Wave Guide in $\eta\to 0$ EM Field

4.1.1 $\{\Psi_1,\Psi_4\}$ *FEM Model Solution* $\mathcal{E}'_0 < 0$:

A W′xL′=.4x18 FEM 2-D bar (Fig.(2b) inset) is driven on the upfield end surface by a uniform loading(with A=1) via Eq.(19) into Eq.(22) (e.g. Fig.(1) driver @ N_c=6) while using the **3.4** model parameters.

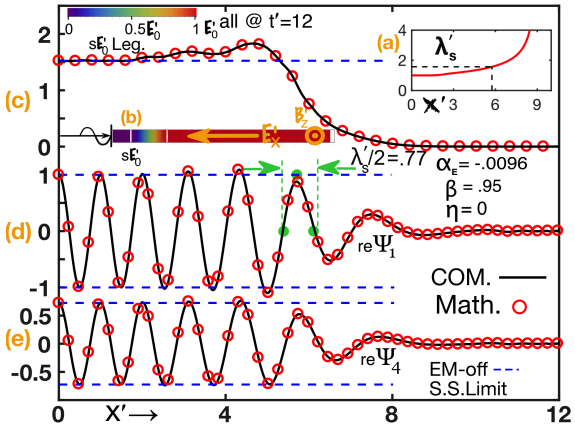

Figure 2. $\{\Psi_1,\Psi_4\}$ PW Passes Thru $\mathcal{E}'_0 < 0$ EM Field

Unlike the Ref.[4] static electric or magnetic fields that varied with only one spatial coordinate, here the Eqs.(12a-b) vary with both (x',y') thus not allowing simple PW solutions. Therefore we start with the simplest situation where the traveling EM spatial wave length is extremely long (take limit $\eta\to 0$, thus $\tilde{\omega}'\to 0$ and $\tilde{k}'\to 0$ and $\cos(\tilde{k}'y'-\tilde{\omega}'t')\to 1$) so that we can get a simple PW in the x′ direction . The limit is taken after substituting Eqs. (12a-b) into Eqs.(7c-d). The downfield surface is terminated with zero *(ii)* BC and wave guide transverse surfaces use a *(iii)* $\bar{n}\bullet\bar{\nabla}\psi_n(x'_s,y'_s)=0$ BC . The FEM model consist of three zones: (a) startup *free field* zone where $\mathcal{E}'_0=0$; (b) downfield core

zone where electric field $\mathcal{E}'_0$ = constant; and (c) transition zones where $\mathcal{E}'_0$ gradually increases between the (a↔b) zones. This is accomplished by multiplying $\mathcal{E}'_0$ in Eqs.(7a-b) (i.e. after the Eqs. (12a-b) have been substituted into Eqs.(7c-d)) by $s(x'-x'_o)*\mathcal{E}'_0$ where s( ) is the appropriately shifted COMSOL built in step function with cubic $\int$ shaped transition zones. The inset in Fig.(2b) shows the resulting $s*\mathcal{E}'_0$ electric field, where dark navy blue is the free field zone, red is the constant central core and the rainbow colors in-between show the transition zone. A shift value of $x'_o=1$ is used, which defines the starting point of the electric field $\int$ transition. The Eqs.(7a-b) are solved in COMSOL using the *General-Form PDE "time dependent"* module. The Fig.(2) solutions are at a time snapshot t′=12 and the relevant β, α_E, η parameters are labeled on each plot item. Figure (2c) illustrates the rise of the probability density ρ with $\mathcal{E}'_0$ *turned on vs off*. The Figs.(2d-e) show the growth of the individual $\Psi_1(x'),\Psi_4(x')$ functions where an increasing wavelength vs x′ is observed and cross comparison to a Mathematica FEM solution is good. Figure (2a) is a plot of the Eq.(11) centerline wavelength estimate plot. The local half wave length estimate (e.g. using Eq.(11) evaluated @ mid point x′=5.7 between nulls) is approximated with $\lambda'_s/2=.78$ as compared to the Fig.(2d) 0.77 graphical measurement.

4.1.2 $\{\Psi_1,\Psi_4\}$ *FEM Model Solution* $\mathcal{E}'_0 > 0$:

The same Fig.(2) model is solved except here $\mathcal{E}'_0 > 0$

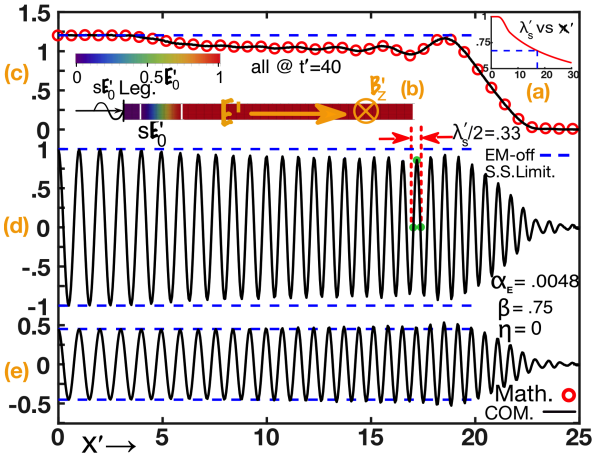

Figure 3. $\{\Psi_1,\Psi_4\}$ PW Passes Thru $\mathcal{E}'_0 > 0$ EM Field

& L′=35, where the Electric field component is in the same direction as the Dirac wave propagation. The Figs.(3d-e) show plots of the $\Psi_1(x'),\Psi_4(x')$ functions where a *decreasing wavelength* vs x′ is observed and the Fig.(3c) ρ vs x′ cross comparison to Mathematica FEM solution is good. Figure (3a) is a plot of the Eq.(11) centerline wavelength estimate. The local half wave length estimate (e.g. using Eq. (11) evaluated @ the mid point x′=17.2 between nulls) is approximated with $\lambda'_s/2=.336$ as compared to the Fig.(3d) 0.334 graphical measurement.

4.2 Simulated PW Thru η>0 EM Field

In lieu of a true PW solution, consider a cylindrical like wave forming after a source is emitted through a slit in an initially EM free zone surrounding the slit and then encounters a transverse traveling η>0 EM wave (Eqs.(13a-b)) as shown in Fig.(4a). The electric field value $s(r'-r'_o)*\mathcal{E}'_0$ is turned on gradually by multiplying it by the COMSOL $\int$ transition step function s( ), with a radial coordinate argument. The slit openings are uniformly driven with the same driver used in the **4.1** bar models. The computed slit centerline $\Psi_1(x')$

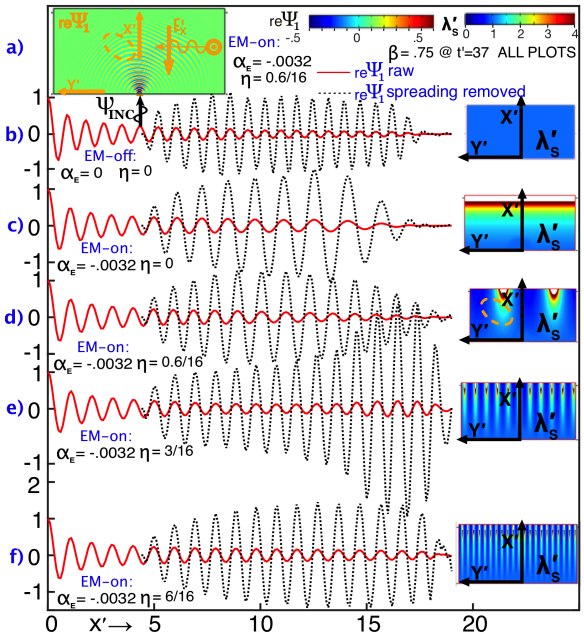

Figure 4. reΨ1 vs x′ for ClyWave Thru EM Field

function is plotted vs x′ @ t′=37 after applying a multiplying factor of $\sqrt{(x'-x_s')}$ to remove the cylindrical spreading, thus simulating a PW propagation scenario. The λ'_s vs (x′,y′) carpet plot insets illustrate where the EM field is likely to alter the free field Dirac waves in the absence of an EM field. For example comparing the dotted zone in Fig.(4a) to the dotted zone in Fig.(4d) inset shows the correspondence between the EM altered Ψ_1 (x′,y′) field and λ'_s field . The Fig.(4c-f) plots illustrate the effect of the EM η traveling wave frequency parameter on reΨ1 (x′,y′) response @ fixed t′=37, as it

is swept through values η={0, .6/16, 3/16, 6/16}. The λ′s vs (x′,y′) inset carpet plots give a sense of the of how the PDE coefficients are being altered by the EM field. Figure (5) keeps the model parameters β=0.75, η=.6/16 the same and examines the effect of varying the EM wave {+y′ or +x′} dir. & ±α_E parameter on $|\Psi_1|$.

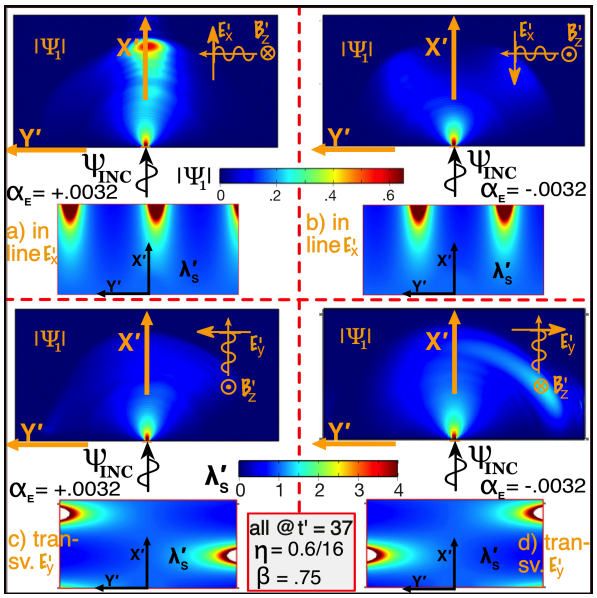

Figure 5. $|\Psi_1|$ vs x′,y′ for ClyWave From Slit Thru EM Field

4.2 Disk Cylindrical Wave Thru EM Field

A (R′o-R′i)xΘ = (16-4)x360° FEM 2-D annular region (e.g. Fig.(6a)) is driven at the inner surface with Eq.(22) while using the Eq.(25) Ref.[2] freely propagating cylindrical Dirac wave (in {r′,θ} cylindrical coordinates @ r′=R′i) for the ψ_n amplitudes and using the labeled β, α_E and η model parameters.The gradual $\mathcal{E}'_0$ buildup is accomplished by multiplying $\mathcal{E}'_0$ in Eqs.(7c-d)

$$\{\psi_1, \psi_4\} \approx \{1,\ exp[i\theta]/\ R'\}exp[ik'_D(r'-R'_i)]/\sqrt{(r'/R'_i)} \quad (25)$$

with $s(r'-r'_o)*\mathcal{E}'_0$ (e.g., Fig.(6e)). Figures (6a-b) give a "$\mathcal{E}'_x$ off" comparison between the Eq.(25) reΨ_4 exact analytical SS limit solution and the Eqs.(7a-b) COMSOL transient solution. Figure (6c) plots Eq.(11) and illustrates how distortions in the Fig.(6d) $\mathcal{E}'_x$ "EM field on" solution, corresponds to the Fig.(6c) λ'_s distortions represented by the dotted A & B comparison zones. Thus pre-solution plots of the $\lambda'_s(x',y',t')$ field gives an idea of where finer mesh zones may be needed before actually making the FEM computer runs. Figures (7a-d) show the Ψ_1,Ψ_4 solutions vs x′ for line cuts at y′=0 @ t′=18. With "EM off," Fig. (7a) shows an exact SS reΨ_1 compared to COMSOL's reΨ_1 for both a step time input (N_c=0) and tapered input (N_c=6) where agreement is good between the SS exact and

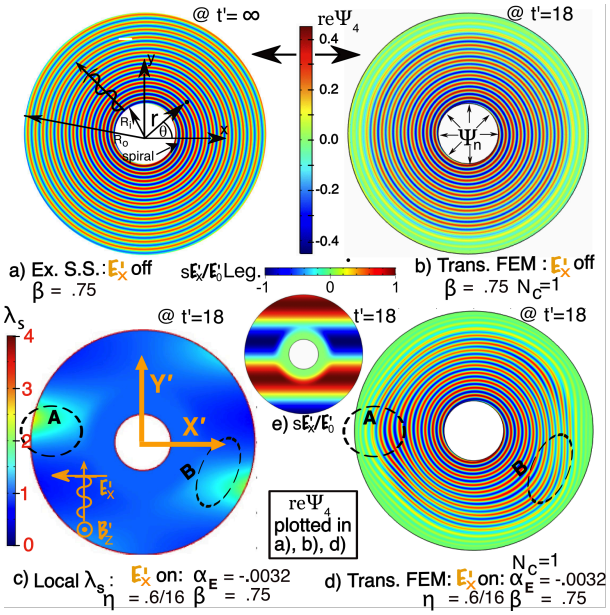

Figure 6. CylW {Ψ_1,Ψ_4} Passes Thru $\mathcal{E}'_0 > 0$ EM Field

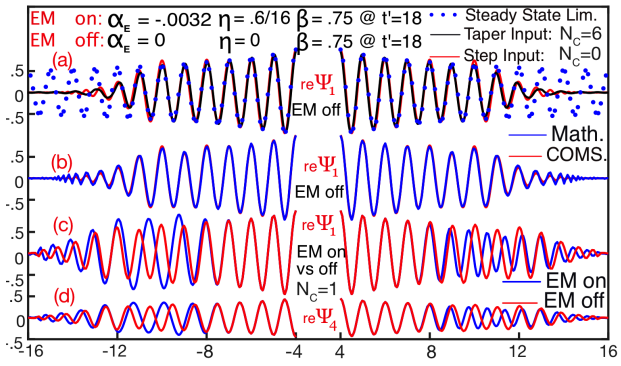

Figure 7. Ψ_1,Ψ_4 vs x′ @ y′=0 at Fig.(6) Section Cuts

FEM solutions. Figure (7b) compares the COMSOL and Mathematica FEM solutions with "EM off" and N_c=0 . Figures (c-d) compare the COMSOL "EM on" vs "EM off" for reΨ_1 and for reΨ_4.

4.3 Two Slit Interference in EM Field

A 2-D 42x21 rectangular FEM model consist of 2 slits of aperture A′p=0.5 and separation P′=5.0 that are embedded in a baffle as shown in the Fig. (8a) "*slit detail*" inset. A (*ii*) zero value BC is used on the downfield surfaces (solutions are terminated before Ψ_n reaches these outer boundaries). It is assumed that the probability of the particle appearing on the back slit wall is negligible so the (*ii*) zero value BC is also used there. The media consist of an existing Eqs.

(12a-b) in line electric field bounded upfield by a circular sector of free field in vacuo media that just encloses the slits as shown in Fig.(8b) inset. Like the previous example, the electric field value $s(r'-r'_o)*\mathcal{E}'_0$ is turned on gradually by multiplying it

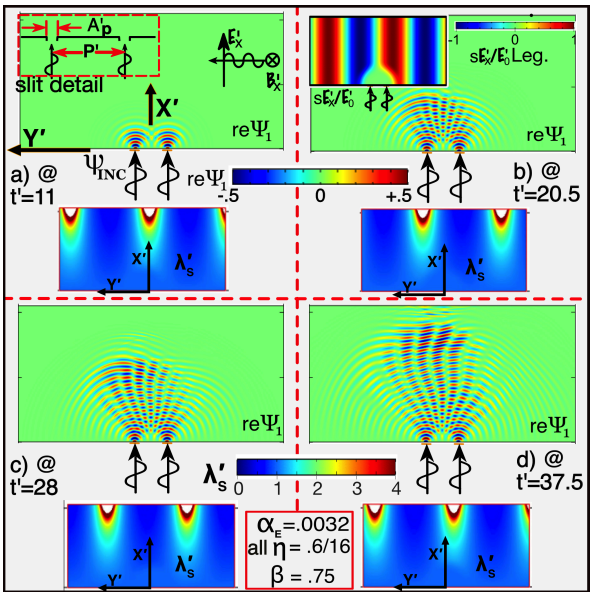

Figure 8. Time History: reΨ$_1$ in EM Field Thru 2 Slits

by the COMSOL∫ transition step function with a radial argument (e.g. Fig.(8b) inset). The slit

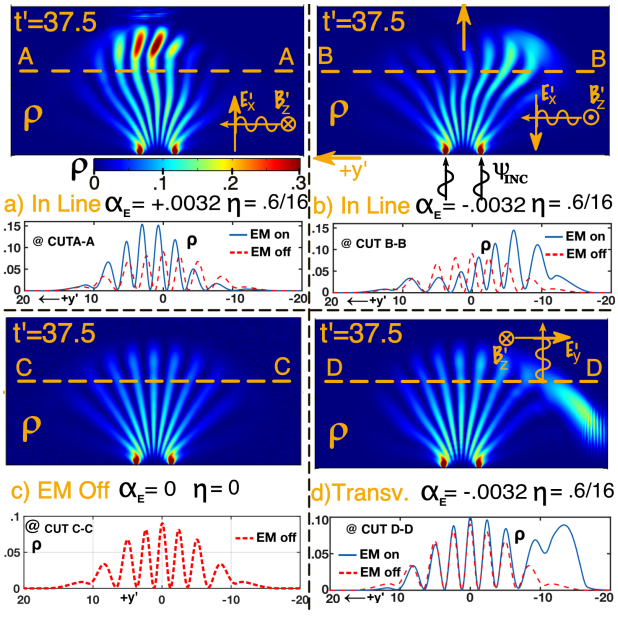

Figure 9. Interference Bands: ρ in EM Field Thru 2 Slits

openings are uniformly driven with the same driver used in the Fig.(5) one slit model. The reΨ$_1$(x′,y′,t′) time history evolvement for an *inline* $\mathcal{E}'_x$ orientation at four time labeled snapshots, is shown respectively in Figs.(8a-d). The classical interference spokes are formed , but get distorted by the EM field. The ρ probability density field, @ t′=37.5 with the EM field turned on in Figs.(9abd) vs off in Fig.(9c), is displayed in upper half of each quadrant of Fig.(9). The " $\mathcal{E}'_x$ off " straight spoke interference patterns of Fig.(9c) are in contrast to the curved spoke interference patterns of Figs.(9abd) . Figure (9b) "in line $\mathcal{E}'_x$" compared to Fig.(9d) "transverse $\mathcal{E}'_y$ " illustrates the effect of the EM wave orientation on the spoke pattern. The lower half of each quadrant in Fig.(9a-d) display line plots (at cuts A-A, B-B, C-C and D-D), which shows interference with EM on vs off.

6. Concluding Remarks

COMSOL successfully solved simultaneous PDEs with spatial and temporal varying coefficients of the type encountered in solving Dirac equations in the presence of a preexisting EM traveling wave. There is good agreement between COMSOL and alternate reference FEM solutions for a long spatial EM wave length relative to the propagating Dirac wavefunction wavelength in a PW waveguide. The free-field Dirac wavefunction tends to be distorted in zones where the k'^2_s (x',y',t') (i.e., the Eq.(11) local steady state PDE coefficient) deviates from the free field wave number squared k'^2_D (actually we track the related $\lambda'_s = re(2\pi/\sqrt{k'^2_s})$. Solutions to the incident harmonic wavefunction upon a two slit barrier entering the EM field, produced curved (rather than straight) c interference band patterns. This paper supersedes the one on file at the time of the Oct. 7, 2020 conference week proceedings.

7. References

[1] A.J. Kalinowski,"Relativistic Quantum Dirac … Equation", COMSOL Conf. Proc., 2016.

[2] A.J. Kalinowski,"Time Dependent Dirac … Mechanics", COMSOL Conf. Proc., 2017.

[3] A.J. Kalinowski,"Relativistic Quantum Mechanical … Magnetic Fields", COMSOL Conf. Proc. 2018.

[4] A.J. Kalinowski,"Growth of Transient Quantum… Fields", COMSOL Conf. Proc., 2019.

[5] Paul Strange, Relativistic Quantum Mechanics, Camb. Univ. Press Cambridge 1998.

[6] Herbert Neff, "Basic Electromagnetic Fields", 2nd edition, Harper & Row, New York.